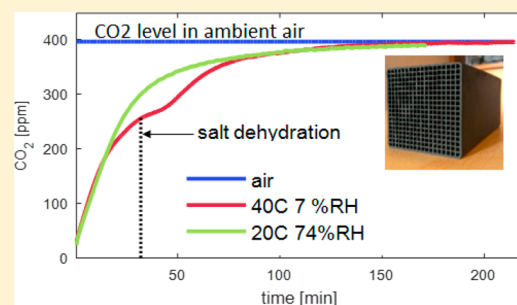# Parametrical Study on CO$_2$ Capture from Ambient Air Using Hydrated K$_2$CO$_3$ Supported on an Activated Carbon Honeycomb

Rafael Rodríguez-Mosqueda,* Eddy A. Bramer, Timo Roestenberg, and Gerrit Brem

Department of Thermal Engineering, Faculty of Engineering Technology, University of Twente, Drienerlolaan 5, 7500 AE Enschede, The Netherlands

S *Supporting Information*

ABSTRACT: Potassium carbonate is a highly hygroscopic salt, and this aspect becomes important for CO$_2$ capture from ambient air. Moreover, CO$_2$ capture from ambient air requires adsorbents with a very low pressure drop. In the present work an activated carbon honeycomb monolith was coated with K$_2$CO$_3$, and it was treated with moist N$_2$ to hydrate it. Its CO$_2$ capture capacity was studied as a function of the temperature, the water content of the air, and the air flow rate, following a factorial design of experiments. It was found that the water vapor content in the air had the largest influence on the CO$_2$ adsorption capacity. Moreover, the deliquescent character of K$_2$CO$_3$ led to the formation of an aqueous solution in the pores of the carrier, which regulated the temperature of the CO$_2$ adsorption. The transition between the anhydrous and the hydrated forms of potassium carbonate was studied by means of FT-IR spectroscopy. It can be concluded that hydrated potassium carbonate is a promising and cheap alternative for CO$_2$ capture from ambient air for the production of CO$_2$-enriched air or for the synthesis of solar fuels, such as methanol.

1. INTRODUCTION

Mankind is approaching the point of no return with respect to the consequences that the increased global warming effect will bring in the future. CO$_2$ capture has been mainly focused on application in power plants;[1−6] nevertheless, in some cases gas pretreatment is required before the capture unit can cope with it.[7] Recently, capturing CO$_2$ directly from ambient air has gathered much attention in the international community.[8,9] It has the advantage that it deals with any kind of CO$_2$ emissions regardless of the type of source, which is especially important for emissions coming from the transportation sector, where in situ capture units are impractical. Moreover, using CO$_2$ as feedstock for subsequent processes would make its harvesting economically attractive. Possible applications are the production of CO$_2$-enriched air that can be used inside greenhouses to enhance the growth of plants. Alternatively, pure CO$_2$ can be used for the synthesis of methanol by means of solar energy, i.e., solar fuels.

A variety of options have been proposed for capturing CO$_2$ from ambient air, including exchange resins,[10,11] microalgae,[12] amine-based adsorbents,[13−18] alkaline metal-based aqueous and solid adsorbents,[19−22] and metal−organic frameworks (MOF).[23,24] In general, amines have been presented as more attractive adsorbents given their high CO$_2$ capture capacities; however, some chemical or physical instability issues have been reported.[25−27]

CO$_2$ capture from ambient air is characterized by the large volume of air that needs to be treated, given its ironically very low CO$_2$ content, around 400 ppm. Moving large volumes of air through the reactor can bring operational issues; for

instance, using aqueous solutions has the disadvantage that the amount of water lost during the air flush can become prohibitive.[28] In addition, the pressure drop in the reactor should be the lowest possible as the power required for moving the air can render the process unfeasible. An attractive option is the use of honeycomb monoliths given the high surface area they provide with a very low pressure drop. Sakwa-Novak et al.[29] reported an adsorbent composed of an alumina monolith loaded with poly(ethylenimine); the weight loading was 0.3 g$_{amine}$/g$_{ads}$ (g$_{ads}$ denotes grams of adsorbent), and the maximum CO$_2$ capture capacity was 0.7 mmol of CO$_2$/g$_{ads}$, when treated with a dry gas mixture containing 400 ppm of CO$_2$ at 30 °C.

K$_2$CO$_3$ has already been studied as an alternative for capturing CO$_2$ from flue gases; different types of carrier materials have been proposed, among which activated carbon, alumina, and TiO$_2$ have shown the best performances.[30−37] Alumina has the disadvantage that it forms a byproduct with the salt.[38] Primer studies on capturing atmospheric CO$_2$ using K$_2$CO$_3$ supported over alumina or yttrium oxide showed that in order to keep a stable adsorption capacity the regeneration must be carried at 150 °C.[20,21]

Potassium carbonate is a very hygroscopic salt; it hydrates forming the potassium carbonate sesquihydrate, K$_2$CO$_3$·1.5H$_2$O, as indicated by reaction R1. The transition between the anhydrous and the sesquihydrate was reported to happen in
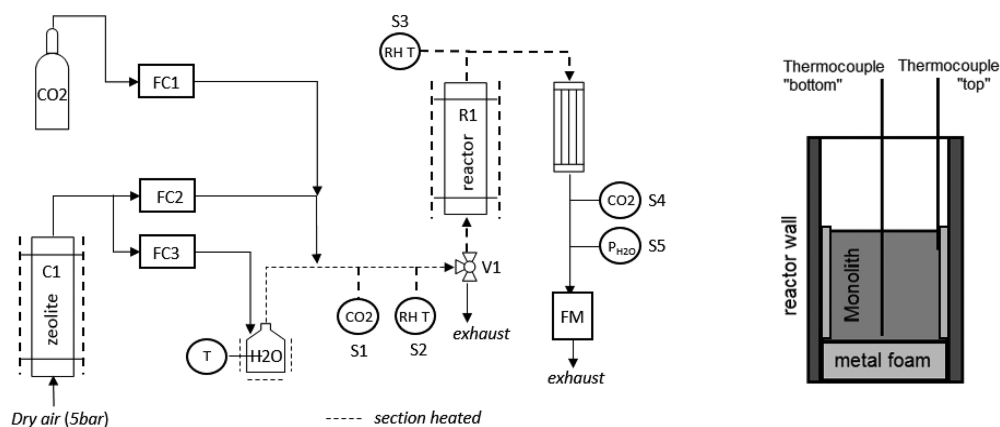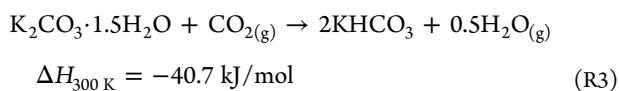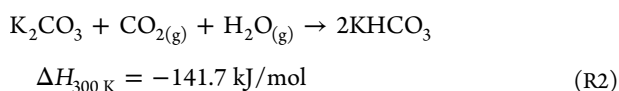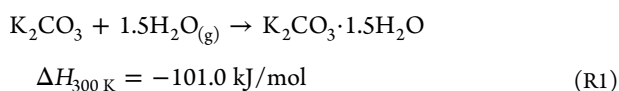
Figure 1. Diagram of the experimental setup (left) and location of the thermocouples inside the reactor (right).

the range from 6 to 10% relative humidity (RH) at 25 °C,[39] and further increase above 43% RH results in the formation of an aqueous solution due to deliquescence.[40] Both carbonates, anhydrous and hydrated, are prone to react with CO_2, forming potassium bicarbonate ($KHCO_3$), as shown by reactions R2 and R3 (all $\Delta H_{300\,K}$ values from ref 41):

$$K_2CO_3 + 1.5H_2O_{(g)} \rightarrow K_2CO_3 \cdot 1.5H_2O$$

$$\Delta H_{300\,K} = -101.0 \text{ kJ/mol} \tag{R1}$$

$$K_2CO_3 + CO_{2(g)} + H_2O_{(g)} \rightarrow 2KHCO_3$$

$$\Delta H_{300\,K} = -141.7 \text{ kJ/mol} \tag{R2}$$

$$K_2CO_3 \cdot 1.5H_2O + CO_{2(g)} \rightarrow 2KHCO_3 + 0.5H_2O_{(g)}$$

$$\Delta H_{300\,K} = -40.7 \text{ kJ/mol} \tag{R3}$$

Theoretical equilibrium calculations by Duan et al.[41] showed the anhydrous carbonate to be more reactive than the hydrate. On the other hand, it is less energy intensive to regenerate $KHCO_3$ back to $K_2CO_3 \cdot 1.5H_2O$ given the lower ΔH of reaction. As indicated in reaction R3, $K_2CO_3 \cdot 1.5H_2O$ can be regenerated from $KHCO_3$ by addition of water. Therefore, it can be proposed to perform the regeneration step via a moisture swing process. In addition, it has been concluded in previous works that a treatment with H_2O before the CO_2 adsorption is advantageous for the CO_2 capture from simulated flue gas.[42,43]

In the present work, a CO_2 adsorbent composed of a monolithic activated carbon honeycomb (ACHC) carrier coated with potassium carbonate was tested for CO_2 capture from ambient air after pretreatment with H_2O. A fractional factorial design of experiments[44] was followed to investigate the effect of the adsorption temperature (T), water vapor pressure of the air (P_w), and volumetric air flow rate (F) on the CO_2 capture capacity of the adsorbent. Finally, one cycle run carrying the regeneration of the adsorbent with a moisture swing at mild temperature is presented to test the feasibility of the process.

2. MATERIALS AND METHODS

2.1. Preparation of the Adsorbent. The activated carbon honeycomb monoliths were purchased from COMELT S.p.A. An activated carbon honeycomb monolith of dimensions 2.9 × 2.9 × 3.0 cm (11 × 11 channels) was dried in an oven at 120

°C for 8 h; the resulting dry mass was 10.65 g. After cooling to room temperature, it was immersed in 120 g of an aqueous solution prepared with a weight ratio of 1 g of K_2CO_3 (Sigma-Aldrich, >99.0%) per 8 g of demineralized water. The immersion was prolonged until no more air bubbles were released from the solution. Afterward, the monolith was shaken manually to remove all excess solution remaining in the channels, and it was calcined in the experimental setup at 170 °C with a flush of dry N_2 to convert all the salt into K_2CO_3. The salt loading was calculated from the increase of the adsorbent's weight over the preparation method. The final weight registered was 11.28 g, which resulted in a salt loading of 0.0558 $g_{K_2CO_3}/g_{ads}$ (5.58 wt %).

2.2. Characterization Techniques. The samples were analyzed using X-ray diffraction, FT-IR spectroscopy, SEM, and BET N_2 adsorption−desorption techniques. A standard X-ray diffractometer (PANalytical X'Pert Pro Powder) equipped with a copper anode X-ray tube was used for the phase identification using Joint Committee Powder Diffraction Standards (JCPDS). An FT-IR spectrometer (PerkinElmer Spectrum 100 FT-IR equipped with a Universal ATR sampling accessory) was used to obtain the infrared spectra. The samples were observed in a SEM microscope (Jeol JSM-6400). The surface area of the activated carbon carrier was calculated based on N_2 adsorption data collected with a Micromeretics ASAP 2400 apparatus, using the BET theory[45] and the pore volume using the BJH theory.[46]

2.3. Experimental Setup. The scheme of the experimental setup is shown in Figure 1. It consists of a fixed bed reactor (R1) of square cross section with dimensions 5 × 5 × 20 cm, while the gas is fed at the bottom of the reactor. A plate is placed at the inlet of the reactor to distribute the flow. The adsorbent is placed on top of a metal foam to further ensure a uniform flow distribution. Metal foams wrapped in aluminum foil are placed between the adsorbent and the inner walls of the reactor to prevent gas bypassing (see right-hand side of Figure 1). Two thermocouples are inserted from the top of the reactor and go through the honeycomb at two locations: at the top and bottom parts, as depicted on the right-hand side of Figure 1. The gas stream fed to the reactor varied among experiments from N_2 to air (400 ppm CO_2), either dry or humid. The air stream was prepared by passing dry air at a pressure of 5 bar through column C1, filled with zeolite 13X beads that removed all CO_2 in it. The flow coming out of the column was divided in two flows controlled by means of controllers FC2 and FC3. The water was added by bubbling one of these flows through

the water reservoir kept at a constant temperature. The CO_2 (Linde, ≥99.7 vol %) addition was controlled by flow controller FC1. Before each experiment the gas mixture prepared was left to stabilize, meanwhile exiting the system from valve V1 below the reactor R1. Once the gas mixture measured remained stable, valve V1 was switched, feeding the reactor. The concentrations of CO_2 and H_2O in the feed stream were measured using sensor S1 (PP Systems SBA-5 CO_2) and sensor S2 (Omega HX92A coupled with a thermocouple), respectively. The CO_2 content in the stream exiting the reactor was measured with sensor S4 (LI-COR LI-820). The humidity content in the stream exiting the reactor was measured at two points: immediately after the reactor with sensor S3 (Omega HX92A coupled with a thermocouple) and after the condensation system by means of sensor S5 (PP systems SBA-5 CO_2/H_2O). The total volumetric flow rate was measured at the exhaust by means of a flowmeter FM (DryCal Mesa Labs Defender 520). Calibration of the CO_2 sensors was checked throughout the experimental set.

2.4. Hydration Experiments. The water uptake by the activated carbon carrier and the adsorbent was tested at 40 °C under a flow of N_2 with different moisture contents, up to 80% RH. The experiments were run until the water vapor pressure in the reactor's outlet equaled the level in the inlet side. The H_2O uptake, H_2O_{ads} [g_{H_2O}/g_{solid}], was calculated from the weight change of the sample with respect to its dry weight.

$$H_2O_{ads} = (m_{final} - m_{dry})/m_{dry}$$

where m_{final} is the mass of the sample measured after the experiment was finished and m_{dry} is the mass of the dry sample.

Also, in the interest of identifying the formation of $K_2CO_3 \cdot 1.5H_2O$, a few milligrams of K_2CO_3 was heated in an oven up to 160 °C and then treated with moist N_2 at 40 °C, varying the humidity content up to 20% RH. The products were analyzed by means of FT-IR spectroscopy to follow any phase change.

2.5. CO_2 Adsorption Experiments. For the study of the CO_2 adsorption capacity, the experimental route consisted of an initial calcination at 170 °C with N_2. Then the cycles were run as follows: humidification, adsorption, and calcination of the adsorbent. The humidification was performed at 40 °C under a flush of 5 L/min of N_2 with a moisture content of P_w = 40 mbar (53% RH) for 2 h. Following the hydration, a CO_2 adsorption experiment was performed under the conditions specified in Table 1 (not in the order shown). The regeneration of the adsorbent was realized by calcining it at 170 °C under a flush of 5 L/min of dry N_2. It has been reported that $KHCO_3$ decomposes quickly and completely above 120 °C.[47]

The CO_2 adsorption capacity [$mmol/g_{ads}$] was calculated as

$$\text{capacity } CO_2 = \frac{F_{n\,air}}{m_{ads}} \int (CO_{2\,in} - CO_{2\,out})\, dt$$

where $F_{n\,air}$ is the molar flow rate of air (dry) at the exhaust of the experimental setup, m_{ads} is the mass of the adsorbent, $CO_{2\,in}$ and $CO_{2\,out}$ are the concentrations of CO_2 in the inlet and outlet of the reactor, and t is the time.

A blank cycle was run using an activated carbon monolith without any K_2CO_3 to test the CO_2 uptake by the carrier. It was observed that no CO_2 was captured as the outlet concentration equaled the inlet value immediately.

The effects of T, P_w, and F on the CO_2 adsorption capacity were investigated following a fractional factorial design of experiments. The ranges tested were as follows: temperature from 20 to 40 °C, water vapor pressure from 5 to 17 mbar, and air flow rate from 5 to 15 L/min. The experiments were performed in a random way so to avoid dependence on the conditions of previous runs. The center point corresponds to the condition at which each of the factors were set at or close to its middle value; those were T = 30 °C, P_w = 12 mbar, and F = 10 L/min. This point was used to investigate the presence of curvature in the response of the adsorption capacity. The repeatability of the results was evaluated by running the center point in triplicate. The experimental conditions used are listed in Table 1 and represented in a cube plot in Figure S1 (see Supporting Information). The CO_2 adsorption capacity data were analyzed using Minitab Statistical Software Version 17.

A desorption experiment was performed with a moisture and temperature swing. For this, a longer adsorbent was prepared using a 6 cm long monolith. The preparation method was the same as described in section 2.1. The salt loading achieved was 0.052 $g_{K_2CO_3}/g_{ads}$. The adsorbent was hydrated and fed with 15 L/min air (400 ppm of CO_2) at 30 °C and P_w = 12 mbar. The desorption test was performed at 65 °C and P_w = 75 mbar under 4 L/min of air (400 ppm of CO_2). The adsorbent was first heated up to the desorption temperature, and then valve V1 was switched. The complete regeneration of the adsorbent was achieved by further calcination under N_2 at 170 °C.

3. CHARACTERIZATION OF THE ADSORBENT

Figure 2 shows the X-ray diffractograms of the activated carbon carrier, the adsorbent, and the adsorbent after the hydration treatment at 40 °C and 53% RH. The loading of the salt over the carrier was corroborated from the presence of reflections characteristic of $K_2CO_3 \cdot 1.5H_2O$. The low intensity of these reflections is explained due to the low amount of salt loaded in the carrier, 5.58 wt %. The rest of the peaks corresponded to distinct phases in the carrier, such as carbon and SiO_2.

Figure 3 shows the SEM pictures of the activated carbon carrier. As seen in Figure 3a, the channels are of square geometry with a length of 1.979 ± 0.006 mm per side, and the wall thickness between the channels is 0.651 ± 0.022 mm. Figure 3b shows the surface of the inner walls of the channels; they looked homogeneous.

The BET surface area of the carrier was 729 m^2/g. The micropore volume calculated with the t-plot method was 0.29 cm^3/g, while the total pore volume in the range of diameters from 1.7 to 300 nm was 0.12 cm^3/g, as determined with the BJH method.

Table 1. Experimental Conditions Tested with Coded Units in Parentheses

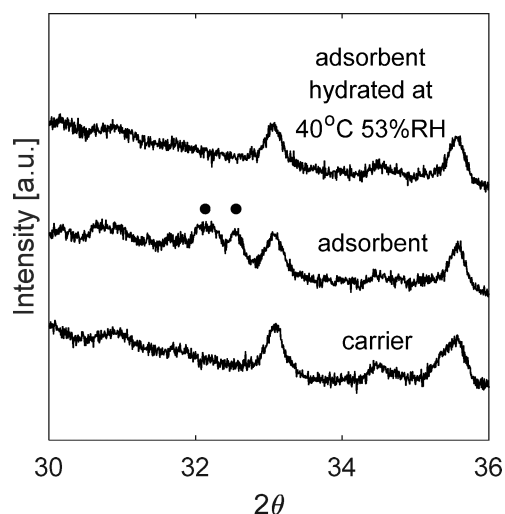| T [°C]	P_w [mbar]	F [L/min]
20 (−1)	5 (−1)	5 (−1)
20 (−1)	5 (−1)	15 (1)
20 (−1)	17 (1)	5 (−1)
20 (−1)	17 (1)	15 (1)
40 (1)	5 (−1)	5 (−1)
40 (1)	5 (−1)	15 (1)
40 (1)	17 (1)	5 (−1)
40 (1)	17 (1)	15 (1)
30 (0)	12 (0)	10 (0)

Figure 2. XRD of the carrier, the adsorbent, and the adsorbent after hydration at 40 °C and 53% RH. (●) $K_2CO_3 \cdot 1.5H_2O$.
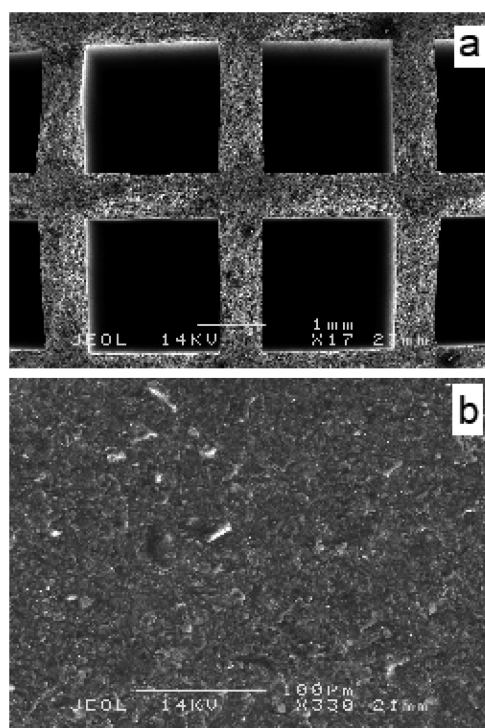

Figure 3. SEM pictures of the activated carbon carrier: (a) view of the channel arrangement; (b) surface of a channel wall.

4. RESULTS OF THE HYDRATION EXPERIMENTS

It has been reported that K_2CO_3 starts to hydrate at 25 °C when the relative humidity is somewhere in the range from 6 to 10% RH and that it deliquesces above 40% RH.[39] The latter observation is in line with the empirical model proposed by Greenspan[40] which indicates that the relative humidity of saturated solutions of K_2CO_3 is around 43% RH, in the temperature range from 10 to 30 °C.

The water adsorption capacities at 40 °C for the carrier and the adsorbent are shown in Figure 4. The uptake by the activated carbon carrier increased sharply at 60% RH, reaching a maximum of 23% weight gain at 80% RH. The uptake at 20% RH for the adsorbent was 4.1 wt %; this is 3 wt % higher than
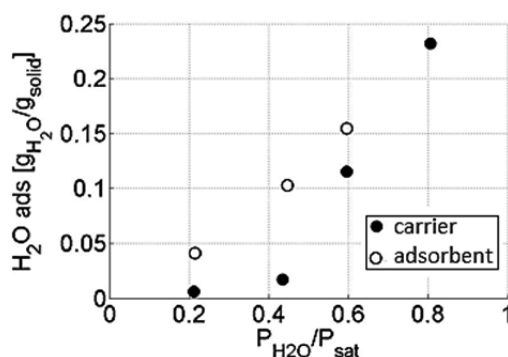

Figure 4. Water uptake by the carrier and the adsorbent at different RH at 40 °C.

the carrier. With respect to the salt loading of 5.58 wt %, the water uptake required to completely convert K_2CO_3 into $K_2CO_3 \cdot 1.5H_2O$ is 1 wt %, indicating that the salt was entirely hydrated. The largest difference between the water uptakes of the samples was seen for the condition at 44% RH. There, the adsorbent's uptake is almost 6 times that of the carrier, and foremost, it is much higher than the theoretically required amount for the formation of $K_2CO_3 \cdot 1.5H_2O$. The reason for this significant difference is that the salt deliquesces at around 43% RH, and therefore all the excess water condensed in the pores of the carrier material producing an aqueous solution of the salt. Finally, the water adsorption capacities of the two samples were not very different above 60% RH. For the CO_2 adsorption cycles from the design of experiments set, the hydration step was performed at 40 °C and 53% RH; the average water uptake for these tests was 12.5 wt %. Figure 2 shows the XRD of the adsorbent after hydration at 40 °C and 53% RH; no reflections corresponding to K_2CO_3 or $K_2CO_3 \cdot 1.5H_2O$ appeared. It is concluded that this treatment with H_2O produced an aqueous solution of K_2CO_3 in the pores of the carrier material, losing the crystalline structure, making it not visible in the diffractograms.

The salt hydration was investigated by means of infrared spectroscopy. Figure 5 shows the spectra of a K_2CO_3 sample subjected to different relative humidity conditions at 40 °C under a flush of N_2. It is noticed that the sample dried in air at 160 °C presented only the peaks corresponding to the anhydrous carbonate ion, CO_3^{-2}: out-of-plane bending at 879
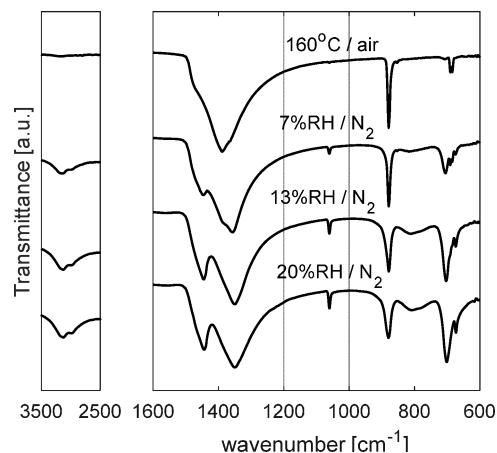

Figure 5. FT-IR spectra of dry K_2CO_3 and under different relative humidties in N_2 at 40 °C.

cm^{-1}, asymmetric stretching at 1400 cm^{-1}, and in-plane bending at 686 cm^{-1}.[48] When the salt was subjected to increasing humidity conditions, the spectrum changed significantly. At 7% RH the initial peaks corresponding to the anhydrous carbonate were still present, although the strongest peak at 1400 cm^{-1} was now a shoulder and new peaks appeared at 1449, 1350, 1060, and 704 cm^{-1}. Even though it was not possible to assign the type of vibration that corresponds to each of these signals, they all fall in the range where C–O vibrations are seen. In particular, it has been found that only hydrated carbonates show a peak at around 1060 cm^{-1} owing to the change of symmetry of the carbonate ion.[49] Additionally, wide peaks appeared at 3000 cm^{-1} due to vibrational modes of water. With further increase of the relative humidity, the peak at 1400 cm^{-1} from the anhydrous carbonate was completely lost at 20% RH.

5. RESULTS OF THE CO$_2$ ADSORPTION EXPERIMENTS

5.1. CO$_2$ Breakthrough during the Adsorption Experiments. Once the hydration treatment was completed, the reactor was fed with a gas stream mimicking ambient air with 400 ppm of CO$_2$ at specific temperature and relative humidity conditions. Figure 6 shows the CO$_2$ breakthroughs for the
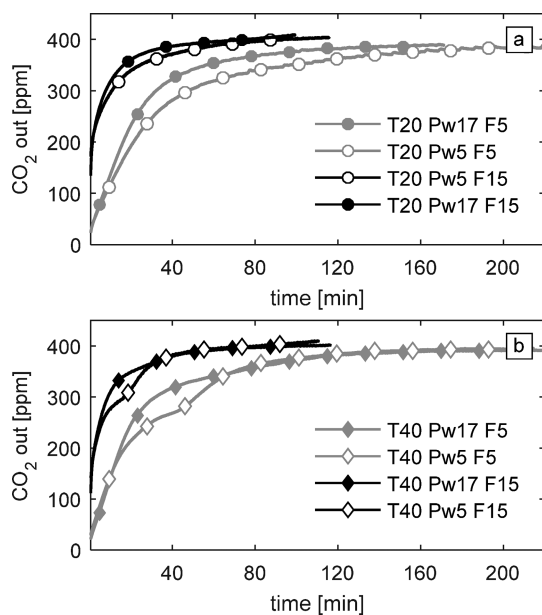

Figure 6. CO$_2$ breakthroughs for the experiments at (a) 20 °C and (b) 40 °C.

experiments listed in Table 1, except for the center point triplicate. It is noticeable that for both adsorption temperatures the lines paired depending on the flow rate. The CO$_2$ capture at 5 L/min reached the lowest CO$_2$ concentration in the outlet. This lower outlet CO$_2$ concentration is a consequence of a longer residence time of the gas in the reactor. Looking at the experiments done at 40 °C, shown in Figure 6b, those performed with P_w = 5 mbar presented an odd shape in the form of a two-step adsorption process. The reason for this behavior is discussed in more detail in section 6.4.

For the sake of making a direct comparison among the different adsorption experiments the cumulative CO$_2$ adsorption capacity is plotted in Figure 7. There the slopes of the lines show qualitatively the rate at which CO$_2$ was adsorbed. Again,
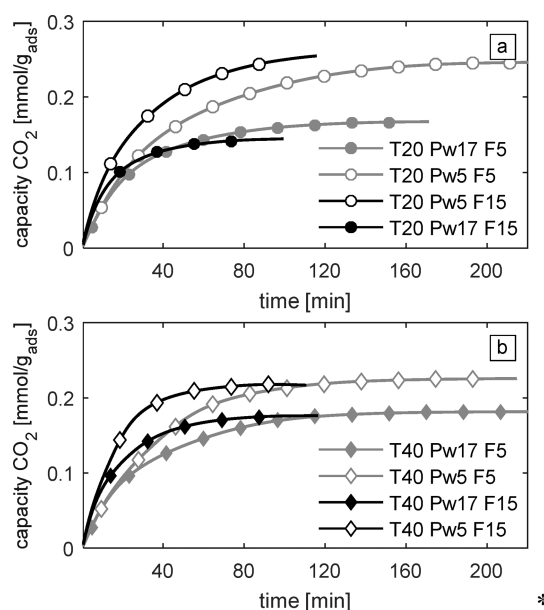

Figure 7. Cumulative capture capacity for adsorptions at (a) 20 °C and (b) 40 °C.

the lines paired during the first 15 min depending on the flow rate used; in general, the adsorbent got saturated after 80–120 min when the flow rate was 15 L/min, and it took more than 150 min when the flow rate was 5 L/min.

Figure 8 shows the adsorption capacities for the different tests. The highest adsorption capacity of 0.249 mmol CO$_2$/g$_{ads}$
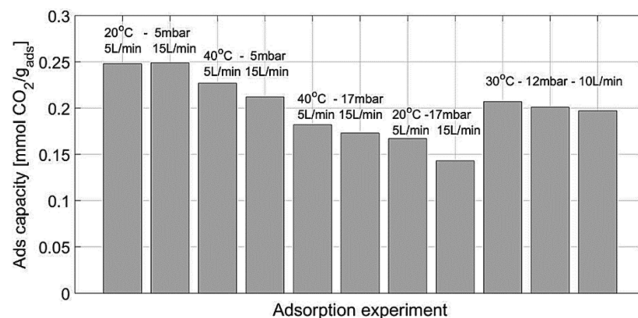

Figure 8. CO$_2$ adsorption capacities from the design of experiments set.

(61.6% salt conversion) was reached for the experiments run at 20 °C and P_w = 5 mbar, and it was independent of the flow rate. On the other hand, the lowest adsorption capacity of 0.143 mmol CO$_2$/g$_{ads}$ (35.4% salt conversion) was obtained at 20 °C, P_w = 17 mbar, and 15 L/min. It was reported in a previous work by Zhao et al.[50] that an adsorbent composed of activated carbon particles, loaded with 4.43 wt % K$_2$CO$_3$, was completely converted into KHCO$_3$ at 20 °C and P_w = 20 mbar under 10 000 ppm of CO$_2$. This indicates the influence of the CO$_2$ partial pressure on the total salt conversion. Furthermore, the capture capacity of our adsorbent was lower than the 0.7 mmol CO$_2$/g$_{ads}$ reported by Sakwa-Novak et al.[29] for their amine-based adsorbent. However, the difference in the active compound loading is also significant: 30.5 wt % for their poly(ethylenimine) and 5.58 wt % for our current K$_2$CO$_3$-based adsorbent. In this work, it was not possible to reach higher salt loadings on the activated carbon carrier as this led to rather

unstable adsorbents that got destroyed after a few cycles. Moreover, it is not the ultimate objective of this work to reach the highest CO_2 capture capacity, but to investigate the underlying mechanism and the influence of various parameters on the CO_2 capture performance. Certainly, stronger carriers should allow to reach higher capture capacities; increasing the salt loading is one of the principal improvements required in future work.

The triplicate of the center points showed a decrease in the capacity in the order of 0.207, 0.201, and 0.197 mmol CO_2/g_{ads} for the first, middle, and last experiment, respectively, indicating that the adsorbent lost 4.8% of its initial capacity. This capacity loss could be due to some physical deterioration observed in the form of crumbling into a very fine dust.

5.2. Statistical Analysis of the CO_2 Capture Capacity Data.
The adsorption capacity data were further analyzed using Minitab Statistical Software version 17 to determine the influence of the T, P_w, and F factors as well as any interaction effect among them. The output is a statistical model to predict the adsorption capacity for a given set of T, P_w, and F conditions. The fitted equation (E1) in normalized or coded units (a coded unit sets −1, 0, and 1 to the lowest, middle, and highest values of a given factor, respectively) was

$$\text{capacity [mmol CO}_2/\text{g}_{ads}] = -0.034 P_w - 0.006 F$$
$$+ 0.013 (TP_w) + 0.200 \qquad (E1)$$

The standard deviation is 0.006 mmol CO_2/g_{ads} (this represents 4.2% of the lowest adsorption capacity measured), and R^2 is 97.85%, indicating a good fit. As seen from eq E1, the capture capacity is defined by P_w, F, and the interaction TP_w. The sign and magnitude of the coefficients show that water vapor pressure has the largest negative influence on the capacity, and the flow rate has only a slightly negative effect. The temperature−water pressure interaction has a positive effect in the capture capacity. An important aspect to point out is the absence of a term for the temperature itself as it could be expected that it should have the largest negative influence in the CO_2 capture due to shifting of the chemical equilibrium. Moreover, opposite to previous works, increasing P_w did not have a beneficial effect on the capture capacity.[42,51,52]

Figure 9 shows the main effects plot for each of the factors studied; the capture capacity varies linearly in the window of conditions tested, as the average of the center point triplicate falls in the lines predicted by the linear model.

Regarding the interaction among the factors, only $T−P_w$ has a considerable influence while $T−F$ and $P_w−F$ do not have a noticeable effect. Figure 10 shows the $T−P_w$ interaction plot,
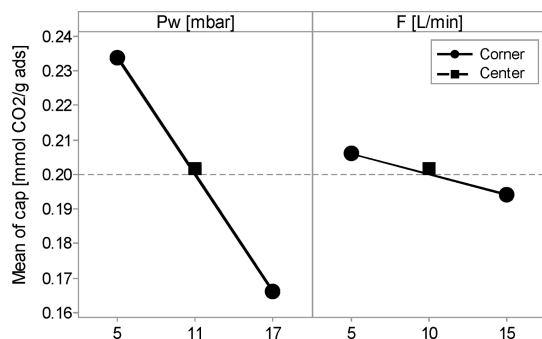
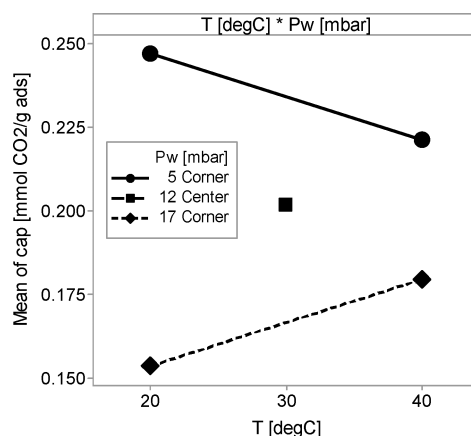**Figure 9.** Main effects plot for the capture capacity data.

Figure 10. $T−P_w$ interaction plot for the capture capacity data.

where an opposite behavior can be seen at lower and higher P_w. At high P_w the capture capacity increases with temperature; on the other hand, at low P_w it decreases with temperature. Nevertheless, lower P_w resulted in better adsorption performances for any temperature.

It seemed rather inconsistent that higher temperatures could somehow result in a better CO_2 capture performance. It could be expected that for the chemical equilibrium of an exothermic process, such as CO_2 adsorption, an increase of temperature is detrimental for the conversion. However, repetition of experiments with P_w = 17 mbar at both 20 and 40 °C and for both flows led to the same results. To elucidate the reasons for this trend, as well as for the magnitude of each the coefficients in the statistical model, the evolution of P_w and T throughout the experiments and the effect of F are discussed in detail in the next sections.

6. DISCUSSION

6.1. Evolution of the Water Vapor Pressure during the Adsorption Experiments.
The water vapor pressure measured in the outlet of the reactor during the adsorption experiments is shown in Figure 11. It is seen in Figure 11b that
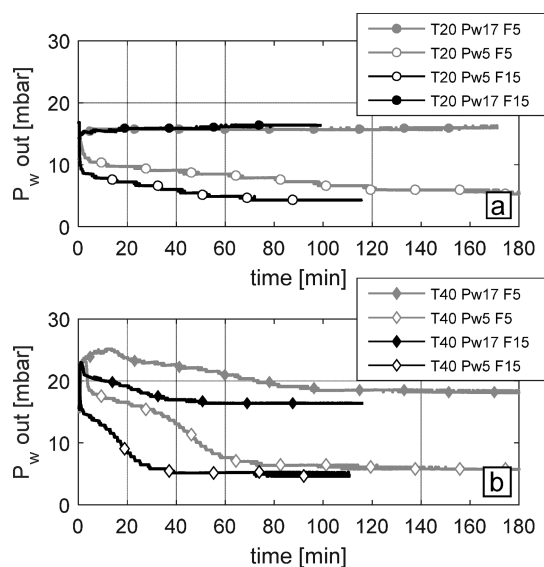
Figure 11. P_w at the outlet of the reactor during the CO_2 adsorption experiments at (a) 20 °C and (b) 40 °C.
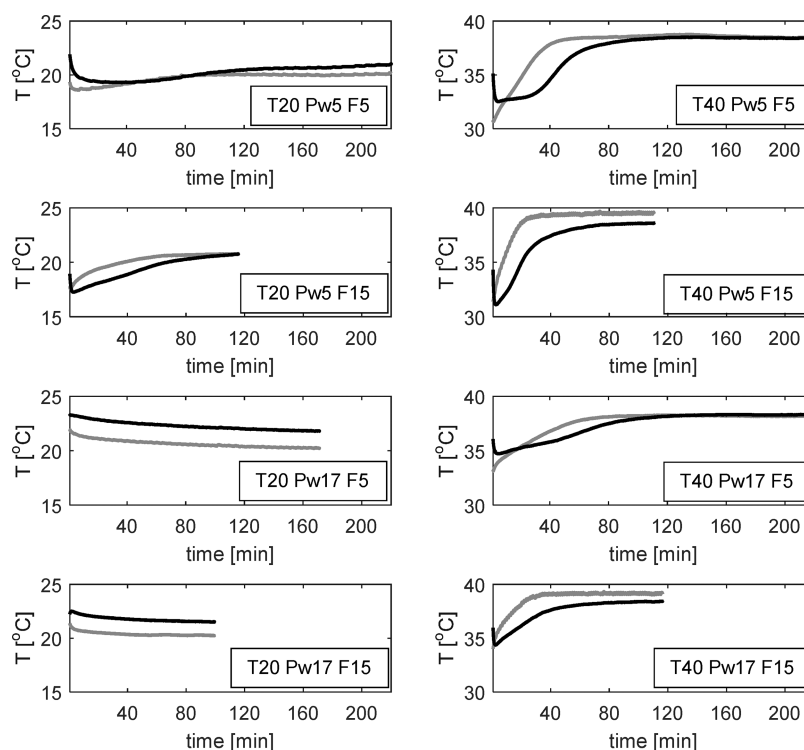
Figure 12. Temperature profiles in the reactor during the CO_2 adsorption. Left-hand side: at 20 °C. Right-hand side: at 40 °C. Gray line: "bottom" location; black line: "top" location.

for all the experiments performed at 40 °C the adsorbent evaporated water into the air stream as the moisture content at the outlet was higher than the inlet level of either 5 or 17 mbar. For the experiments performed at 20 °C, Figure 11a shows that at P_w = 5 mbar water evaporation occurred, while at P_w = 17 mbar a slight uptake can be noticed.

To explain the behavior in each experiment, four possible subprocesses that either consume or release water can be proposed; three of them are related to the potassium salt, and a fourth one is associated with the activated carbon carrier. Those related with the salt are (i) adsorption or evaporation of water according to the water vapor equilibrium of the aqueous solution of the salt, (ii) release of water due to the carbonation of $K_2CO_3 \cdot 1.5H_2O$, as indicated in reaction R3, and (iii) release of water from the dehydration of $K_2CO_3 \cdot 1.5H_2O$. Regarding the activated carbon carrier, (iv) uptake or release of water depending on its water adsorption equilibrium, shown in Figure 4.

With respect to the first process listed, it was concluded that the hydration pretreatment at 53% RH led to the formation of an aqueous solution of the salt in the pores. Since the saturation pressure of this solution is 43% RH, if the air stream supplied has a lower relative humidity, the solution will evaporate H_2O to counteract this condition. This is the case for all experiments performed at 40 °C and that at 20 °C and P_w = 5 mbar. This also explains why the experiments run at 20 °C and 17 mbar did not evaporate any water as this corresponds to 74% RH. The product of this evaporation will be $K_2CO_3 \cdot 1.5H_2O$, provided that the relative humidity does not go below the vapor pressure of the sesquihydrate. It should be noticed that the aqueous solution of the salt, present from the beginning, can capture CO_2 as well. Concerning the second and third processes mentioned, even though CO_2 is indeed being captured, the amount of water released during the carbonation

of $K_2CO_3 \cdot 1.5H_2O$ is just 1 mol of H_2O per two of CO_2 captured. Thus, even in the case of removing all CO_2 from the airstream only 0.2 mbar of H_2O (200 ppm) would be released into it; the profiles show much larger water releases. It is not likely that $K_2CO_3 \cdot 1.5H_2O$ dehydrated as the relative humidity in all the experiments is above 10% RH, except in the case of the experiments run at 40 °C and P_w = 5 mbar, with approximately 7% RH. The CO_2 breakthrough of those cases shows a two-step adsorption process, which is attributed to the dehydration of $K_2CO_3 \cdot 1.5H_2O$. In any case the amount of water released during the adsorption experiment is much larger than the water released by complete dehydration of the sesquihydrate.

The results seem to contradict the findings of previous works in the sense that a higher P_w during the adsorption resulted in a better CO_2 capture performance.[31,42,43] Those studies included a pretreatment of the K_2CO_3/AC adsorbent with water, resulting in the conversion of the salt into $K_2CO_3 \cdot 1.5H_2O$, and then the CO_2 capture was performed under CO_2 contents higher than 400 ppm. At first sight, it seems contradictory that increasing the water content in the gas stream would be beneficial for the carbonation of the sesquihydrate. In fact, this is already indicated by the chemical reaction (R3) where water is on the right side, inhibiting the carbonation. It has been proposed that higher humidities lead to the formation of a quasi-liquid interface that enhances the transport of reactants and thus favors the carbonation.[53]

6.2. Evolution of Temperature in the Reactor. In principle, CO_2 adsorption is an exothermic process; however, it can be expected that the overall evolution of heat will be determined by either the adsorption or desorption of water from the adsorbent. This is due to that this happened in a larger extent, but parallel to the CO_2 capture. Figure 12 shows the temperatures measured at the "bottom" and "top" locations.

Looking at the graphs on the left-hand side, experiments at 20 °C, only experiments with P_w = 5 mbar show a slight initial cooling effect of approximately 3 °C, and then the temperature slowly raises until the set point. In contrast, the experiments run with P_w = 17 mbar show an initial slight temperature increase and then a decrease until the set point. These temperature evolutions match well with the trends of P_w in the outlet of the reactor shown in Figure 11. The cooling is linked to the water evaporation, and the slight warming is caused by the adsorption of water. Regarding the experiments run at 40 °C, depicted on the right-hand side of Figure 12, a cooling effect is occurring in all the cases. The largest drop in temperature, of about 8 °C, is seen for P_w = 5 mbar and a temperature decrease of around 5 °C for P_w = 17 mbar. This larger temperature drop compared to the experiments at 20 °C is explained by the fact that the evaporation rate of water is much faster at 40 °C than at 20 °C. Moreover, the adsorbent starts to cool at the entrance of the channel, and if the relative humidity of this stream is not 43% RH yet, the adsorbent will keep cooling in the direction of the flow along the channel length, resulting in the temperature profiles seen.

This cooling effect can also explain why the temperature did not appear in the statistical model. The relative humidity conditions of the incoming air determine if water will evaporate from the adsorbent, and this process regulates the temperature locally. The $T-P_w$ interaction buffers the effect of a higher inlet temperature. This is a rather important characteristic of the adsorbent as it makes it possible to capture CO_2 from ambient air in warm places where the local temperature might, in principle, be inconvenient for the process. For instance, in a real application it is proposed to regenerate the adsorbent by converting $KHCO_3$ back to $K_2CO_3 \cdot 1.5H_2O$ and further formation of the aqueous solution via a moisture swing process, therefore resulting in an adsorbent loaded with an excess of water that will function as coolant in a subsequent adsorption step.

Nonetheless, this cooling effect does not explain why the experiments at P_w = 17 mbar perform better at 40 °C than at 20 °C. To explain this, the effect of a higher temperature on the diffusion of components in a gaseous mixture needs to be considered. The local cooling of the adsorbent is much larger for the experiments at 40 °C than at 20 °C. Therefore, the temperature difference of the adsorbent's surface among these experiments was not 20 °C, but less as shown in Figure 12. It might be that the adsorbent's surface was cooler than measured by the thermocouples as those were inserted throughout the channels; i.e., they were not directly over the adsorbent's surface. For this reason, it is possible that the CO_2 concentration just next to the adsorbent's surface, i.e. interphase, is not very distinct among these experiments. However, the temperature in the bulk of the gas stream should be closer to the set point conditions. Then, the diffusion of CO_2 from the bulk of the gas will be favored by a hotter bulk temperature,[54] ultimately enhancing the CO_2 capture.

6.3. Effect of the Flow Rate on the Adsorption Capacity.
The flow rate had the lowest influence of all the parameters included in the statistical model (E1). It was reported previously that increasing the flow rate was beneficial in getting higher adsorption capacities with faster rates. However, above certain flow the adsorption capacity drops again. This has been attributed to a shorter contact time of the gas with the adsorbent's surface for larger flows.[42,43,55]

6.4. Phase Transition of the Sesquihydrate.
The CO_2 breakthrough curves showing a two-step capture profile were seen for experiments at 40 °C and P_w = 5 mbar; those correspond to a relative humidity of around 7% RH. However, there was a large temperature drop inside the reactor, increasing the relative humidity locally. In Figure 13 the
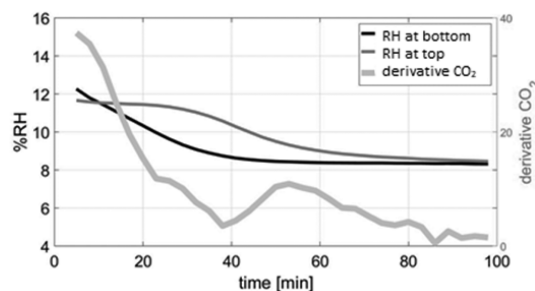

Figure 13. Relative humidity inside the reactor and derivative of the CO_2 in the outlet.

relative humidity calculated from the temperature measured at the "bottom" and "top" locations inside the reactor is plotted against the derivative of the CO_2 concentration in the outlet. Showing the derivative rather than the concentration itself gives a better impression of the change in the CO_2 adsorption performance. It is observed that the derivative drops from the start of the experiment and rises again before reaching 40 min, indicating a reactivation of the CO_2 adsorption. The relative humidity at the inflection point is 8.8% RH and 10.8% RH at the "bottom" and "top" locations, respectively. It was mentioned that previous theoretical studies showed anhydrous K_2CO_3 to be more reactive with CO_2.[41] This two-step behavior suggests the dehydration of $K_2CO_3 \cdot 1.5H_2O$. Figure 14 shows
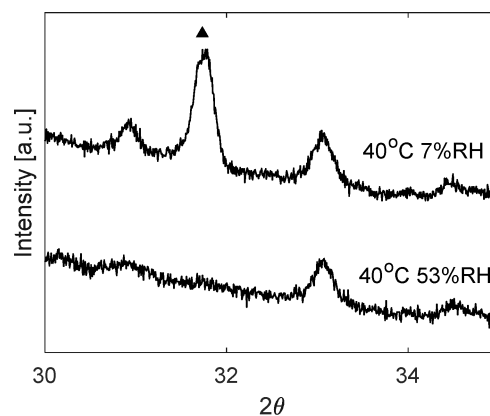

Figure 14. XRD of the adsorbent hydrated at 40 °C and 53% RH and after exposition at 40 °C and 7% RH, both in N_2. (▲) K_2CO_3.

the diffractograms of the adsorbent hydrated at 40 °C and 53% RH in N_2, and after a subsequent treatment at 40 °C and 7% RH in N_2, the formation of anhydrous K_2CO_3 is corroborated. To support this hypothesis, an adsorption experiment was run at the same conditions, but without prior hydration of the adsorbent. Figure 15 shows that the CO_2 breakthrough of the sample not hydrated was a one-step process as the reaction happening is the direct carbonation of K_2CO_3.

It should be noted that there is not a unique mechanism for the CO_2 capture by hydrated K_2CO_3. According to the experiments performed, an aqueous solution of the salt was
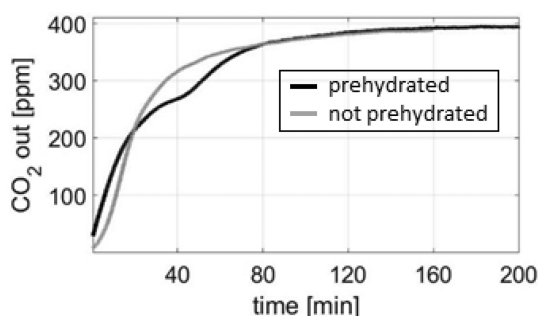
Figure 15. CO_2 breakthrough at 40 °C, P_{H_2O} = 5 mbar, and 5 L/min.

deposited over the pores of the carrier. Part of this solution acted as the CO_2 adsorbent, and the other part was evaporated, leaving $K_2CO_3 \cdot 1.5H_2O$. If the relative humidity of the incoming air was below the stability level for the sesquihydrate, it dried to K_2CO_3. Both $K_2CO_3 \cdot 1.5H_2O$ and K_2CO_3 were able to capture CO_2 as well, within the T and P_w ranges tested.

7. REGENERATION OF THE ADSORBENT VIA A MOISTURE SWING AT MILD TEMPERATURE

Finally, a desorption experiment was performed via a moisture swing at mild temperature to regenerate the $KHCO_3$ back to $K_2CO_3 \cdot 1.5H_2O$. Regeneration steps at elevated temperatures and under a flow of N_2 will have a large energy penalty, making the process not economically feasible. The desorption experiment was performed at 65 °C and P_w = 75 mbar under an air flush (400 ppm of CO_2) of 4 L/min. This method allows to obtain CO_2-enriched air streams that can be used in greenhouses. Figure 16 shows that the CO_2 concentration
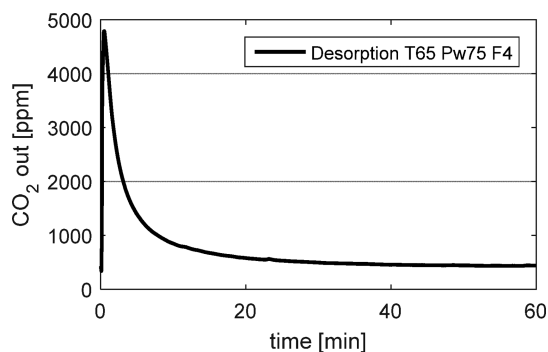

Figure 16. Desorption test at 65 °C and P_w = 75 mbar under F = 4 L/min air with 400 ppm of CO_2.

peak was just below 5000 ppm. The mass balance showed that 50% of the total CO_2 captured was released in the experiment. Even though the maximum CO_2 concentration was not high enough for a practical application (e.g., 1% CO_2), this experiment proved the concept of cycling between $K_2CO_3 \cdot 1.5H_2O$ and $KHCO_3$. Further optimization of the desorption process is required.

8. CONCLUSIONS

The results showed that CO_2 can be removed from ambient air using an adsorbent composed of potassium carbonate supported on an activated carbon honeycomb. Depending on the relative humidity, the supported potassium carbonate takes moisture from the ambient producing potassium carbonate sesquihydrate or an aqueous solution inside the pores of the

carrier. From the hydration treatment performed prior to the CO_2 adsorption, an aqueous solution capable of capturing CO_2 was formed. This solution will evaporate toward $K_2CO_3 \cdot 1.5H_2O$ or K_2CO_3 if the water vapor pressure of the incoming air is below their corresponding equilibrium water vapor pressures. This evaporation induces a local cooling in the adsorbent which is beneficial for the CO_2 adsorption. The influences of the adsorption temperature, the air moisture content, and the air flow rate on the CO_2 capture capacity were studied following a multifactorial design of experiments, showing that the water vapor pressure had the largest influence. The highest capture capacity achieved was 0.249 mmol CO_2/g_{ads}; however, the salt loading was only 0.0558 $g_{K_2CO_3}$/g_{ads}. The salt content was kept rather low due to physical deterioration of the carrier at higher loadings. Sturdier carriers should allow higher salt loadings, resulting in higher capture capacities. Finally, a complete cycle of adsorption and regeneration with a moisture swing at 65 °C and 75 mbar of water vapor produced a peak CO_2 concentration of ca. 5000 ppm, making it an attractive option for application in greenhouses.

■ ASSOCIATED CONTENT

ⓢ Supporting Information

The Supporting Information is available free of charge on the ACS Publications website at DOI: 10.1021/acs.iecr.8b00566.

> Figure S1: cube plot of the parameters of the Design of Experiments (PDF)

■ AUTHOR INFORMATION

Corresponding Author

*E-mail: rf.rodmos@outlook.com or r.rodriguezmosqueda@utwente.nl (R.R.-M.).

ORCID ⓘ

Rafael Rodríguez-Mosqueda: 0000-0001-8201-0277

Author Contributions

The authors thank Henk-Jan Moed, Dominc Post, and Sven van der Heide for their technical contributions. The authors thank staff from Antecy B.V. and Alexander Louwes for the discussion of the results presented.

Notes

The authors declare no competing financial interest.

■ REFERENCES

(1) Creamer, A. E.; Gao, B. Carbon-Based Adsorbents for Postcombustion CO_2 Capture: A Critical Review. *Environ. Sci. Technol.* **2016**, *50* (14), 7276−7289.

(2) Abanades, J. C.; Grasa, G.; Alonso, M.; Rodriguez, N.; Anthony, E. J.; Romeo, L. M. Cost Structure of a Postcombustion CO_2 Capture System Using CaO. *Environ. Sci. Technol.* **2007**, *41* (15), 5523−5527.

(3) Liu, Y.; Ye, Q.; Shen, M.; Shi, J.; Chen, J.; Pan, H.; Shi, Y. Carbon Dioxide Capture by Functionalized Solid Amine Sorbents with

Simulated Flue Gas Conditions. *Environ. Sci. Technol.* **2011**, *45* (13), 5710−5716.

(4) Nagy, T.; Mizsey, P. Effect of Fossil Fuels on the Parameters of CO_2 Capture. *Environ. Sci. Technol.* **2013**, *47* (15), 8948−8954.

(5) Babarao, R.; Jiang, Y.; Medhekar, N. V. Postcombustion CO_2 Capture in Functionalized Porous Coordination Networks. *J. Phys. Chem. C* **2013**, *117* (51), 26976−26987.

(6) Yu, J.; Balbuena, P. B. Water Effects on Postcombustion CO_2 Capture in Mg-MOF-74. *J. Phys. Chem. C* **2013**, *117* (7), 3383−3388.

(7) Lackner, K. S. Capture of carbon dioxide from ambient air. *Eur. Phys. J.: Spec. Top.* **2009**, *176*, 93−106.

(8) Sanz-Pérez, E. S.; Murdock, C. R.; Didas, S. A.; Jones, C. W. Direct Capture of CO_2 from Ambient Air. *Chem. Rev.* **2016**, *116* (19), 11840−11876.

(9) Zeman, F. Energy and Material Balance of CO_2 Capture from Ambient Air. *Environ. Sci. Technol.* **2007**, *41* (21), 7558−7563.

(10) Wang, T.; Lackner, K. S.; Wright, A. Moisture Swing Sorbent for Carbon Dioxide Capture from Ambient Air. *Environ. Sci. Technol.* **2011**, *45* (15), 6670−6675.

(11) Chen, Z.; Deng, S.; Wei, H.; Wang, B.; Huang, J.; Yu, G. Polyethylenimine-Impregnated Resin for High CO_2 Adsorption: An Efficient Adsorbent for CO_2 Capture from Simulated Flue Gas and Ambient Air. *ACS Appl. Mater. Interfaces* **2013**, *5* (15), 6937−6945.

(12) Brilman, W.; Alba, L. G.; Veneman, R. Capturing atmospheric CO_2 using supported amine sorbents for microalgae cultivation. *Biomass Bioenergy* **2013**, *53*, 39−47.

(13) Brilman, W. F.; Veneman, R. Capturing Atmospheric CO_2 Using Supported Amine Sorbents. *Energy Procedia* **2013**, *37*, 6070−6078.

(14) Chaikittisilp, W.; Khunsupat, R.; Chen, T. T.; Jones, C. W. Poly(allylamine)−Mesoporous Silica Composite Materials for CO_2 Capture from Simulated Flue Gas or Ambient Air. *Ind. Eng. Chem. Res.* **2011**, *50* (24), 14203−14210.

(15) Belmabkhout, Y.; Serna-Guerrero, R.; Sayari, A. Amine-bearing mesoporous silica for CO_2 removal from dry and humid air. *Chem. Eng. Sci.* **2010**, *65*, 3695−3698.

(16) Choi, S.; Gray, M. L.; Jones, C. W. Amine-Tethered Solid Adsorbents Coupling High Adsorption Capacity and Regenerability for CO_2 Capture From Ambient Air. *ChemSusChem* **2011**, *4*, 628−635.

(17) Wurzbacher, J. A.; Gebald, C.; Piatkowski, N.; Steinfeld, A. Concurrent Separation of CO_2 and H_2O from Air by a Temperature-Vacuum Swing Adsorption/Desorption Cycle. *Environ. Sci. Technol.* **2012**, *46* (16), 9191−9198.

(18) Gebald, C.; Wurzbacher, J. A.; Tingaut, P.; Zimmermann, T.; Steinfeld, A. Amine-Based Nanofibrillated Cellulose As Adsorbent for CO_2 Capture from Air. *Environ. Sci. Technol.* **2011**, *45* (20), 9101−9108.

(19) Holmes, G.; Nold, K.; Walsh, T.; Heidel, K.; Henderson, M. A.; Ritchie, J.; Klavins, P.; Singh, A.; Keith, D. W. Outdoor Prototype Results for Direct Atmospheric Capture of Carbon Dioxide. *Energy Procedia* **2013**, *37*, 6079−6095.

(20) Veselovskaya, J. V.; Derevschikov, V. S.; Kardash, T. Y.; Stonkus, O. A.; Trubitsina, T. A.; Okunev, A. G. Direct CO_2 capture from ambient air using K_2CO_3/Al_2O_3 composite sorbent. *Int. J. Greenhouse Gas Control* **2013**, *17*, 332−340.

(21) Derevschikov, V. S.; Veselovskaya, J. V.; Kardash, T. Y.; Trubitsyn, D. A.; Okunev, A. G. Direct CO_2 capture from ambient air using K_2CO_3/Y_2O_3 composite sorbent. *Fuel* **2014**, *127*, 212−218.

(22) Zeman, F. Reducing the Cost of Ca-Based Direct Air Capture of CO_2. *Environ. Sci. Technol.* **2014**, *48* (19), 11730−11735.

(23) McDonald; Lee; Mason; Wiers; Hong; Long. Capture of carbon dioxide from air and flue gas in the alkylamine-appended metal-organic framework mmen-Mg2(dobpdc). *J. Am. Chem. Soc.* **2012**, *134* (16), 7056−7065.

(24) Bhatt, P. M.; Belmabkhout, Y.; Cadiau, A.; Adil, K.; Shekhah, O.; Shkurenko, A.; Barbour, L. J.; Eddaoudi, M. A Fine-Tuned Fluorinated MOF Addresses the Needs for Trace CO_2 Removal and Air Capture Using Physisorption. *J. Am. Chem. Soc.* **2016**, *138* (29), 9301−9307.

(25) Jindaratsamee, P.; Shimoyama, Y.; Ito, A. Amine/glycol liquid membranes for CO_2 recovery form air. *J. Membr. Sci.* **2011**, *385−386*, 171−176.

(26) Wagner, A.; Steen, B.; Johansson, G.; Zanghellini, E.; Jacobsson, P.; Johansson, P. Carbon Dioxide Capture from Ambient Air Using Amine-Grafted Mesoporous Adsorbents. *Int. J. Spectrosc.* **2013**, *2013*, 1.

(27) Gebald, C.; Wurzbacher, J. A.; Tingaut, P.; Steinfeld, A. Stability of Amine-Functionalized Cellulose during Temperature-Vacuum-Swing Cycling for CO_2 Capture from Air. *Environ. Sci. Technol.* **2013**, *47* (17), 10063−10070.

(28) Stolaroff, J. K.; Keith, D. W.; Lowry, G. V. Carbon Dioxide Capture from Atmospheric Air Using Sodium Hydroxide Spray. *Environ. Sci. Technol.* **2008**, *42* (8), 2728−2735.

(29) Sakwa-Novak, M. A.; Yoo, C. J.; Tan, S.; Rashidi, F.; Jones, C. W. Poly(ethylenimine)-Functionalized Monolithic Alumina Honeycomb Adsorbents for CO_2 Capture from Air. *ChemSusChem* **2016**, *9* (14), 1859−68.

(30) Zhao, C.; Chen, X.; Zhao, C. CO_2 Absorption Using Dry Potassium-Based Sorbents with Different Supports. *Energy Fuels* **2009**, *23* (9), 4683−4687.

(31) Sharonov, V. E.; Tyshchishchin, E. A.; Moroz, E. M.; Okunev, A. G.; Aristov, Y. I. Sorption of CO_2 from Humid Gases on Potassium Carbonate Supported by Porous Matrix. *Russ. J. Appl. Chem.* **2001**, *74* (3), 409−413.

(32) Okunev, A.; Sharonov, V.; Aristov, Y.; Parmon, V. Sorption of carbon dioxide from wet gases by K_2CO_3-in-porous matrix: influence of the matrix nature. *React. Kinet. Catal. Lett.* **2000**, *71* (2), 355−362.

(33) Hayashi, H.; Taniuchi, J.; Furuyashiki, N.; Sugiyama, S.; Hirano, S.; Shigemoto, N.; Nonaka, T. Efficient Recovery of Carbon Dioxide from Flue Gases of Coal-Fired Power Plants by Cyclic Fixed-Bed Operations over K_2CO_3-on-Carbon. *Ind. Eng. Chem. Res.* **1998**, *37* (1), 185−191.

(34) Zhao, C.; Guo, Y.; Li, C.; Lu, S. Removal of low concentration CO_2 at ambient temperature using several potassium-based sorbents. *Appl. Energy* **2014**, *124*, 241−247.

(35) Shigemoto, N.; Yanagihara, T.; Sugiyama, S.; Hayashi, H. Material Balance and Energy Consumption for CO_2 Recovery from Moist Flue Gas Employing K2CO3-on-Activated Carbon and Its Evaluation for Practical Adaptation. *Energy Fuels* **2006**, *20* (2), 721−726.

(36) Esmaili, J.; Ehsani, M. Study on the Effect of Preparation Parameters of K2CO3/Al2O3 Sorbent on CO_2 Capture Capacity at Flue Gas Operating Conditions. *J. Encapsulation Adsorpt. Sci.* **2013**, *3* (2), 57−63.

(37) Zhao, C.; Chen, X.; Zhao, C. Carbonation Behavior and the Reaction Kinetic of a New Dry Potassium-Based Sorbent for CO_2 Capture. *Ind. Eng. Chem. Res.* **2012**, *51* (44), 14361−14366.

(38) Lee, S. C.; Choi, B. Y.; Lee, T. J.; Ryu, C. K.; Ahn, Y. S.; Kim, J. C. CO_2 absorption and regeneration of alkali metal-based solid sorbents. *Catal. Today* **2006**, *111*, 385−390.

(39) Wells, M. L.; Wood, D. L.; Sanftleben, R.; Shaw, K.; Hottovy, J.; Weber, T.; Geoffroy, J.-M.; Alkire, T. G.; Emptage, M. R.; Sarabia, R. Potassium carbonate as a dessicant in effervescent tablets. *Int. J. Pharm.* **1997**, *152* (2), 227−235.

(40) Greenspan, L. Humidity Fixed Points of Binary Saturated Aqueous Solutions. *J. Res. Natl. Bur. Stand., Sect. A* **1977**, *81A* (1), 89−96.

(41) Duan, Y.; Luebke, D. R.; Pennline, H. W.; Li, B.; Janik, M. J.; Halley, J. W. Ab Initio Thermodynamic Study of the CO_2 Capture Properties of Potassium Carbonate Sesquihydrate, $K2CO3·1.5H_2O$. *J. Phys. Chem. C* **2012**, *116* (27), 14461−14470.

(42) Lee, S. C.; Chae, H. J.; Choi, B. Y.; Jung, S. Y.; Ryu, C. Y.; Park, J. J.; Baek, J.-I.; Ryu, C. K.; Kim, J. C. The effect of relative humidity on CO_2 capture capacity of potassium-based sorbents. *Korean J. Chem. Eng.* **2011**, *28* (2), 480−486.

(43) Lee, S. C.; Choi, B. Y.; Ryu, C. K.; Ahn, Y. S.; Lee, T. J.; Kim, J. C. The effect of water on the activation and the CO_2 capture capacities

of alkali metal-based sorbents. *Korean J. Chem. Eng.* **2006**, *23* (3), 374−379.

(44) NIST Engineering Statistics Handbook; http://itl.nist.gov/div898/handbook/pri/section3/pri334.htm.

(45) Brunauer, S.; Emmett, P. H.; Teller, E. Adsorption of Gases in Multimolecular Layers. *J. Am. Chem. Soc.* **1938**, *60* (2), 309−319.

(46) Barrett, E. P.; Joyner, L. G.; Halenda, P. P. The Determination of Pore Volume and Area Distributions in Porous Substances. I. Computations from Nitrogen Isotherms. *J. Am. Chem. Soc.* **1951**, *73* (1), 373−380.

(47) Tanaka, H. Comparison of thermal properties and kinetics of decompositions of $NaHCO_3$ and $KHCO_3$. *J. Therm. Anal.* **1987**, *32*, 521−526.

(48) Chasan, D. E.; Norwitz, G. Infrared determination of inorganic sulfates and carbonates by the pellet technique. In Department of the Army Frankford Arsenal, Philadelphia, PA, 1969.

(49) Buijs, K.; Schutte, C. J. H. An infra-red study of the hydrates of sodium carbonate. *Spectrochim. Acta* **1961**, *17* (9), 917−920.

(50) Zhao, C.; Guo, Y.; Li, C.; Lu, S. Carbonation behavior of K_2CO_3/AC in low reaction temperature and CO_2 concentration. *Chem. Eng. J.* **2014**, *254*, 524−530.

(51) Guo, Y.; Zhao, C.; Li, C.; Wu, Y. CO_2 sorption and reaction kinetic performance of K_2CO_3/AC in low temperature and CO_2 concentration. *Chem. Eng. J.* **2015**, *260*, 596−604.

(52) Park, S. W.; Sung, D. H.; Choi, B. S.; Lee, J. W.; Kumazawa, H. Carbonation kinetics of potassium carbonate by carbon dioxide. *J. Ind. Eng. Chem.* **2006**, *12* (4), 522−530.

(53) Tuwati, A.; Fan, M.; Russell, A. G.; Wang, J.; Dacosta, H. F. M. New CO_2 Sorbent Synthesized with Nanoporous $TiO(OH)_2$ and K_2CO_3. *Energy Fuels* **2013**, *27* (12), 7628−7636.

(54) Hirschfelder, J. O.; Bird, R. B.; Spotz, E. L. The Transport Properties of Gases and Gaseous Mixtures. II. *Chem. Rev.* **1949**, *44* (1), 205−231.

(55) Lodewyckx, P.; Van Rompaey, D.; Verhoeven, L.; Vansant, E. F. Water isotherms of activated carbons with small amounts of surface oxygen groups: Fitting the mesopore region. *Carbon* **2001**, *39* (2), 309−310.